TISSUE ENGINEERING: Part C
Volume 17, Number 2, 2011

DOI: 10.1089/ten.tec.2010.0182

Modeling Tissue Growth Within Nonwoven Scaffolds Pores

Sharon L. Edwards, Ph.D.,[1] Jeffrey S. Church, Ph.D.,[1] David L.J. Alexander, Ph.D.,[2] Stephen J. Russell, Ph.D.,[3] Eileen Ingham, Ph.D.,[4] John A.M. Ramshaw, Ph.D.,[5] and Jerome A. Werkmeister, Ph.D.[5]

In this study we present a novel approach for predicting tissue growth within the pores of fibrous tissue engineering scaffolds. Thin nonwoven polyethylene terephthalate scaffolds were prepared to characterize tissue growth within scaffold pores, by mouse NR6 fibroblast cells. On the basis of measurements of tissue lengths at fiber crossovers and along fiber segments, mathematical models were determined during the proliferative phase of cell growth. Tissue growth at fiber crossovers decreased with increasing interfiber angle, with exponential relationships determined on day 6 and 10 of culture. Analysis of tissue growth along fiber segments determined two growth profiles, one with enhanced growth as a result of increased tissue lengths near the fiber crossover, achieved in the latter stage of culture. Derived mathematical models were used in the development of a software program to visualize predicted tissue growth within a pore. This study identifies key pore parameters that contribute toward tissue growth, and suggests models for predicting this growth, based on fibroblast cells. Such models may be used in aiding scaffold design, for optimum pore infiltration during the tissue engineering process.

Introduction

Pore architecture is an important consideration in the design of tissue engineering scaffolds. Pores are void openings that necessarily connect together to form channels through the scaffold. They aid the transportation of nutrients, and waste, in and out of the scaffold,[1] cell migration through the scaffold,[2] and the formation of a coherent tissue as a result of pore infiltration by cells.[3]

Fiber-based scaffolds are commonly used and can be manufactured by, for example, nonwoven,[4–6] electrospinning,[7,8] or fused fiber deposition[9–11] technologies. Within these scaffolds voids between adjacent fibers form pores, with fiber segments representing the pore struts, and crossing fibers, the strut intersections.

Pore features studied in relation to tissue growth include pore size[3,5,11–17] and, more recently, pore geometry.[18] Pore size affects cellular activities such as pore spanning,[3,11,12,15,16] with this ability varying between different cell types,[3] and the spatial organization of cells within pores.[5,14] Cell number can also be affected, with an increase in pore size, often leading to a decrease in scaffold-specific surface area for cell attachment and proliferation.[5,13] The effect of pore geometry on tissue growth has been investigated to a lesser extent, studying its influence on tissue orientation and the pattern of tissue growth within pores.[18]

The principle mechanism by which (fibroblast) cells infiltrate and fill pores generally begins with them gathering at strut intersections[9,12,18,19] and spanning across the smallest interstrut distance. As the cells divide they form a sheet, a few layers thick, consisting of cells embedded within a secreted extracellular matrix (ECM). The cells within the sheet interact with one another, laterally hanging on to each other and adjacent struts,[19] acting as a complex dynamic structure.[12] In cases where cells are uniformly seeded around the pore perimeter, the cell sheet infiltrates the pore circumferentially,[9,18] with the shape of the tissue outline influenced by the pore geometry.[18] Where cells are not uniformly distributed, but collected at the strut intersections, they span the pore successively back and forth across the shortest distance, infiltrating in a noncircumferential manner.[18] Interstrut distances that multilayered fibroblasts can bridge has been reported to be up to 200 μm after a 2-week culture period[12,15,16] and 420 μm after a month,[12] with the ECM becoming more loosely connected with increasing interstrut distance.[11]

In addition to the formation of cell sheets within scaffold pores,[5,6,19,20] clustered cell aggregates have also been reported.[5,6,14,20] Studies suggest that cell sheets generally form within pores where spanning is easy and scaffold surface area is high.[5,6] Conversely, cell aggregates form in large pores, where spanning is difficult and the scaffold surface area is low.[5,6] With differences in cell spatial organization leading to

[1]Materials Science and Engineering, CSIRO, Geelong, Victoria, Australia.
[2]Mathematics Informatics and Statistics, CSIRO, Clayton, Victoria, Australia.
[3]Nonwovens Research Group, School of Design, University of Leeds, Leeds, United Kingdom.
[4]Institute of Molecular and Cellular Biology, University of Leeds, Leeds, United Kingdom.
[5]Molecular and Health Technologies, CSIRO, Clayton, Victoria, Australia.

changes in cell morphology,[5] this can affect cell growth[5,21–23] and, as a consequence, cell function,[5,22] with high levels of differentiation found with restricted cell spreading,[22] such as in large cell aggregates.[5] These studies highlight that a more precise understanding of the influence of pore properties, such as geometry, on cellular activities and tissue formation could lead to tissue engineering scaffolds of improved design. The aim of this study was to correlate tissue growth within fiber-bound scaffold pores with aspects of pore geometry. This was achieved by culturing fibroblast cells on thin nonwoven scaffolds *in vitro*, for measurement of tissue lengths at fiber crossovers and along fiber segments. From these measurements mathematical models were determined and a software program was written to visualize tissue growth, based on derived models. This work provides an approach for improving pore geometry within scaffolds to give enhanced cell growth during pore infiltration, as part of the tissue engineering process. No other known methods of predicting tissue growth in pores based on pore geometry are known by the authors.

Materials and Methods

Scaffold manufacture and characterization

Nonwoven scaffolds were prepared from bicomponent sheath-core polyethylene terephthalate fibers (Huvis) of mean staple length 64 mm and linear density 6.7 decitex (diameter 26 μm). The sheath and core melting points were ~100°C and ~245°C, respectively. After scouring and sterilization these fibers have been observed to have good biocompatibility compared to other fiber types.[4] Prepared parallel-laid carded webs were combed and manually layered to produce structures in which the resulting planar fiber orientation was biaxially anisotropic. Fabrics were thermally stabilized by means of through-air thermal bonding at 130°C, fusing the outer sheath of the fibers at the crossover points, stabilizing the structure without thermal shrinkage.

Standard methods[24,25] were used to characterize manufactured scaffolds ($n = 29$) in terms of thickness and mass per unit area. Scaffold porosity (%) was calculated according to the equation below, where M is the scaffold mass per unit area (g/cm^2), t is the scaffold thickness (cm), and ρ_{fiber} is the fiber density (taken to be 1.38 g/cm^3). All results are expressed as mean ± standard error of the mean.

$$Porosity = 100 \times \left(1 - \frac{M}{t \times \rho_{fiber}}\right)$$

Pore length (major axial length) ($n = 2697$ pores) and fiber segment orientation ($n = 4163$ fiber segments) on the scaffold surface were measured using image analysis software (Image-Pro® Plus; MediaCybernetics).

Cell culture

Scaffolds (15 mm in diameter) were secured in holders (CellCrown; Scaffdex) and sterilized using gamma irradiation (15 kGy; Steritech). Mouse NR6 fibroblast cells (passage 7) were suspended in supplemented Dulbecco's modified Eagle's medium (Gibco®, Invitrogen) at a cell concentration of 6×10^4 cells/mL. Dulbecco's modified Eagle's medium was supplemented with 10% (v/v) fetal calf serum (JRH Biosciences), 1% (v/v) L-glutamine, and 0.5% (v/v) penicillin/streptomycin (5000 units/mL; CSL Biosciences). Cell suspensions (1.5 mL) were statically seeded onto scaffolds, placed in microbiology-grade suspension culture 24-well plates (Cellstar®, Greiner Bio-one, Invitrogen), used to prevent cells preferentially attaching to the wells. A background control of medium only was included. Samples were incubated for up to 22 days, changing the medium every other day.

Biological assays

Cell number was quantified using an MTS assay (CellTiter 96®; Promega), measuring absorbance at 490 nm following the manufacturer's instructions. Before conducting the assay, scaffolds and controls were rinsed with phosphate-buffered saline (PBS; Invitrogen) to remove any nonadherent cells and transferred to fresh wells. Cell proliferation was measured on four replicate scaffolds on days 3, 6, 10, 13, 17, and 22 of culture. Background absorbance was corrected by subtracting the absorbance index of scaffolds (without cells) in the culture medium.

A viability assay (LIVE/DEAD®; Molecular Probes™, Invitrogen) was used to assess cell viability, following the manufacturer's instructions. Scaffolds were rinsed in PBS to remove any nonadherent cells and transferred to fresh wells. Treated samples were assessed using a fluorescent microscope (Eclipse TE2000-U; Nikon) to observe live, calcein AM-stained (green) cells and dead, ethidium homodimer-1-stained (red) cells. The viability assay was conducted on days 3, 6, 10, 13, 17, and 22 of culture.

Cell imaging

Scanning electron microscopy (SEM) was used to observe cell attachment to the scaffold surfaces on day 22 of culture. Scaffolds were rinsed in PBS and fixed in 2.5% (v/v) glutaraldehyde (ProSciTech) in PBS. Samples were rinsed in PBS for 3×20 min, and placed in 1% (v/v) osmium tetroxide (ProSciTech) in PBS for 2 h. Samples were then rinsed in distilled water for 3×20 min and serially dehydrated in 70%, 95%, and 100% ethanol (Sigma Aldrich) for 10 min each. Samples were placed in 1:1 ethanol:hexamethyldisilazane (ProSciTech) for 10 min and finally in pure hexamethyldisilazane for 3×10 min. Samples were left to dry overnight and then chromium coated using a Xenosput 2000 (Dynavac), with micrographs taken at 5 kV using a Phenom Desktop scanning electron microscope (FEI).

Characterization of pore features and tissue growth

Pore characteristics, and aspects of tissue growth within them, were measured from the Live/Dead micrographs obtained on day 6 and 10 of culture, using image analysis software. These time points were chosen as cells were in their proliferative phase, with sufficient quantities of tissue present. Since the scaffolds used in this study were of minimal thickness, and the images studied were planar, pore characteristics and tissue growth have been regarded two-dimensionally. During this analysis the fiber segments forming a pore wall were assumed to be straight, with the angle formed between crossing fibers referred to as the interfiber angle (A) (Fig. 1A).

Analysis of tissue growth at the fiber crossover

The interfiber angle and the tissue length along the line bisecting that angle, the vertex tissue length (v), were measured ($n = 48$ data points for day 6 and $n = 110$ for day 10). Vertex tissue lengths that extended to a fiber boundary were not measured. Fiber segment lengths incident to the fiber crossover were also measured (Fig. 1).

Analysis of tissue growth along the fiber segment

Tissue growth along the fiber segment was characterized by measuring tissue lengths (f) perpendicular to the fiber segment ($n = 116$ data points forming 13 sets for day 6 and $n = 154$ data points forming 26 data sets for day 10). Measurements were made at $\sim 7\,\mu m$ intervals along the fiber segment until reaching the lowest point of tissue growth. The corresponding distance along the fiber segment (FSd) from the fiber crossover was also noted (Fig. 1B). Interfiber angle, vertex tissue length, and fiber segment lengths incident to the tissue growth were also measured.

Regression analysis of tissue growth

Regression analysis was conducted on the variables measured at the fiber crossovers and along the fiber segments, modeling tissue growth at both pore sites. The variables included in each model had statistically significant effects on tissue growth (indicated by their probability values; p-values). Models were chosen that did not include cross terms or higher order terms. They were chosen to have a high coefficient of determination (R^2) value, which is a statistical measure of how well the regression line approximates the real data points. A value of 0 indicates that the variables in the model have no predictive power, whereas a value of 1 indicates the model fits the data points perfectly. The standard error of estimate (SEE) for each model is also reported, indicating the scale of the difference between data points and model values.

Models were validated by the method of cross validation, using the leave one out approach. In brief, one data point was removed from the population at a time and a new model calculated. This new model was then used to predict the removed data point. This was repeated with all data points and the standard error of cross validation (SECV) calculated by combining the errors for each of the data points. In the case of the validation of the model for f, the data was rotated out in sets. Values of SECV close to those of the SEE indicate that models could predict data values outside the model equally well as the data values used in the model.

Visualizing predicted tissue growth within pores

A software program was developed using Matlab® (MathWorks) to aid in the visualization of predicted tissue growth within scaffold pores. The program used the interfiber angles and fiber segment lengths constituting a pore as inputs, and from these simulated pore geometry. Tissue growth within the pore was then predicted based on the models input into software, and compared to actual tissue growth on day 6 of culture. Using models for growth at the fiber crossover and along the fiber segment in conjunction permitted the visualization of complete tissue growth within the pore.

Results

Scaffold properties

The manufacturing method adopted in this study yielded scaffolds with an average thickness and porosity of $114 \pm 7\,\mu m$ and $86\% \pm 1\%$, respectively. Image analysis of the scaffold surface showed a right skewed unimodal distribution for pore major axial length, with a modal value of 26–50 μm. Fiber segments were found to possess an anisotropic orientation.

Cell proliferation and viability

The MTS assay showed that the growth phase, in which cells were in their proliferative state, continued until day 13 of culture, with cell numbers more than doubling between

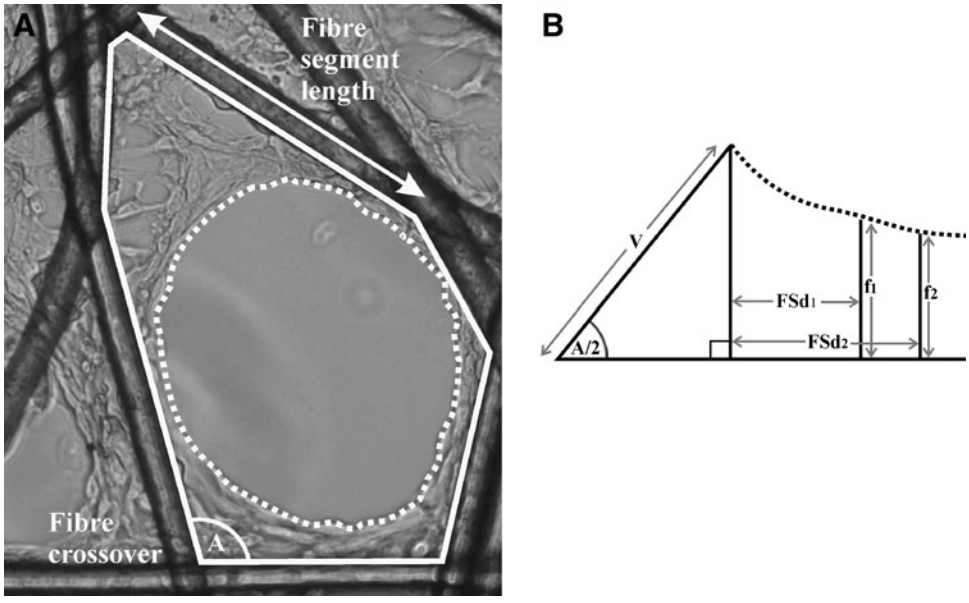

FIG. 1. **(A)** Optical micrograph with illustration of pore outline (solid line) and tissue outline (dashed line), and **(B)** schematic of measured pore characteristics, defining interfiber angle (A), vertex tissue length (v), and tissue length along the fiber segment (f), at corresponding distance (FSd).

day 6 and 10 (data not shown). These results were reflected in the Live/Dead assay (Fig. 2A, B), with almost all of the cells viable. The growth phase was followed by a stationary phase, in which cell numbers remained constant until day 22. This was associated with ECM secretion, as observed in Live/Dead and SEM micrographs (data not shown).

Observations in pore infiltration

Generally, SEM micrographs showed cells to be uniformly distributed around the pore perimeter (Fig. 3A), with preferential spanning at fiber crossovers, where cell-to-cell contact was evident in spanning interfiber distances (Fig. 3B). Cells appeared to be organized as flat sheets, rather than aggregates, often with several cell layers within these sheets. Study of the Live/Dead micrographs revealed the main method of pore infiltration to be circumferential (Fig. 2B). A rarely observed method of infiltration involved cells clustering at a particular point around the pore perimeter, usually at fiber crossovers. From here they bridged the pore using one another to span large distances, filling the pore in a noncircumferential pattern.

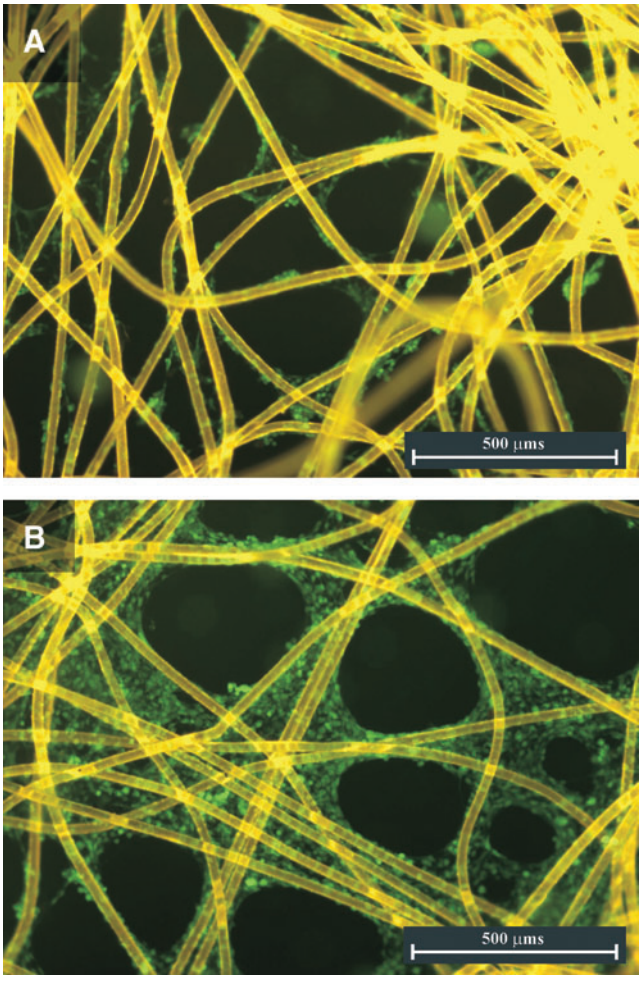

FIG. 2. Live/Dead micrographs showing pore infiltration by viable (green) fibroblasts on **(A)** day 6 and **(B)** day 10 of culture. Color images available online at www.liebertonline.com/ten.

Tissue growth at fiber crossovers

Tissue growth at fiber crossovers decreased with increasing interfiber angle. Analysis of this growth suggested an exponential relationship between the vertex tissue length and the interfiber angle, on both days 6 and 10 of culture (Fig. 4). Confidence intervals (95%) are included for each of the data sets, indicating the expected spread of individual observations according to the models.

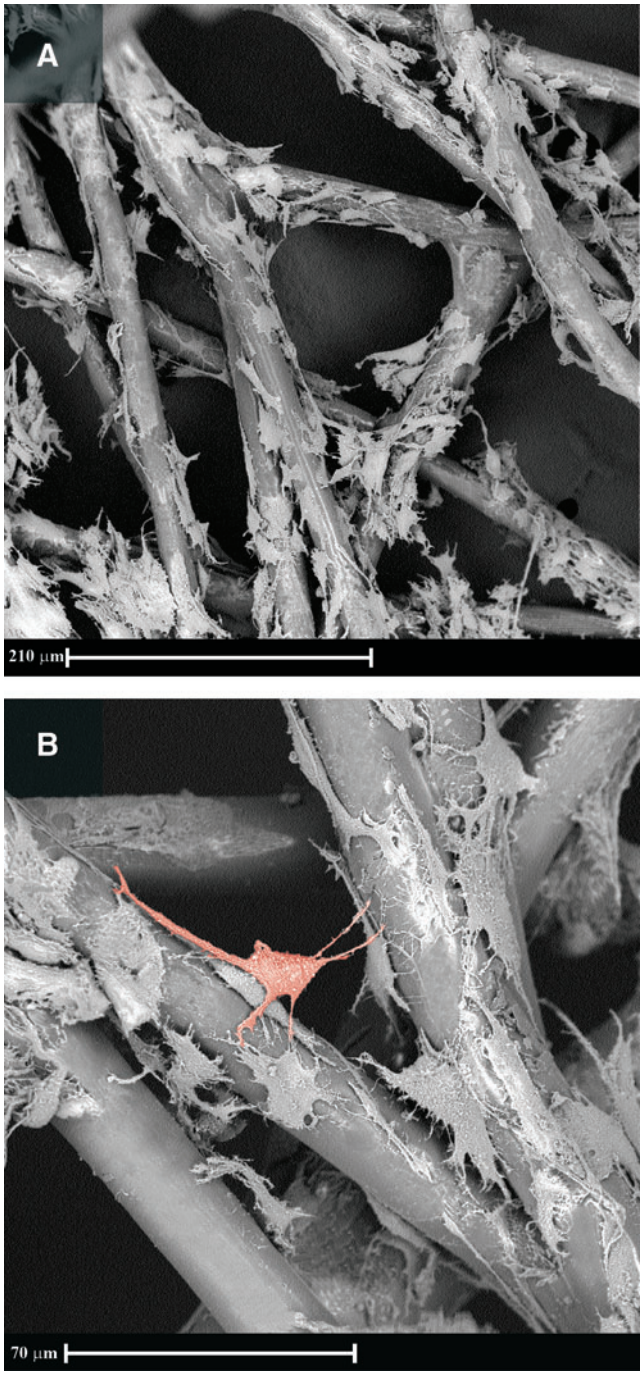

FIG. 3. Scanning electron micrographs of fibroblasts **(A)** around pore perimeter and **(B)** pseudocolored red cell spanning interfiber distance at fiber crossover, on day 22 of culture. Color images available online at www.liebertonline.com/ten.

Exponential models were found to fit better than linear models, with linear regressions giving R^2 values of 0.69 and 0.51 on day 6 and 10, respectively. Models determined for day 6 and day 10 were $\ln(v) = 5.5741 - 0.0153A$ and $\ln(v) = 5.5943 - 0.0146A$, respectively. For day 6 the R^2 value was 0.72 and the SEE was 0.36, whereas for day 10 the R^2 value was 0.54 and the SEE was 0.42. The SECV for day 6 and day 10 models were calculated to be 0.39 and 0.43, respectively. The small SEE, with closely matching SECV indicates the level of accuracy that this model is capable of predicting. Analysis of data sets incorporating the lengths of fiber segments incident to the intersection found no significant effect of fiber segment length in the exponential models for day 6 or 10.

The confidence intervals plotted in Figure 4 revealed a large overlap between day 6 and day 10 tissue lengths, with no significant increase in growth between these time points. This was likely due to cell layering, in the formation of thicker cell sheets, as revealed by SEM and optical microscopy.

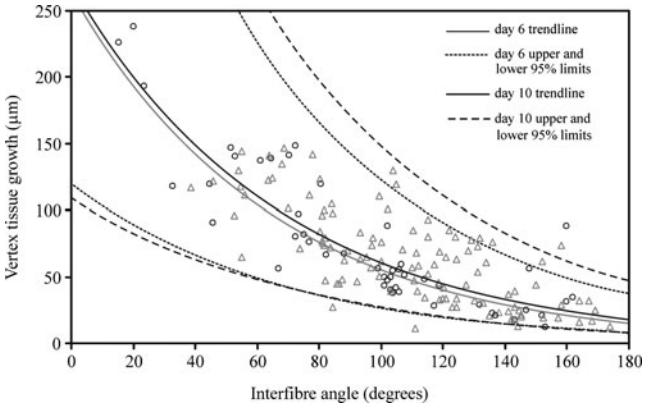

FIG. 4. Vertex tissue length plotted against interfiber angle on day 6 (circles) and day 10 (triangles) of culture, with exponential trendlines and 95% confidence limits.

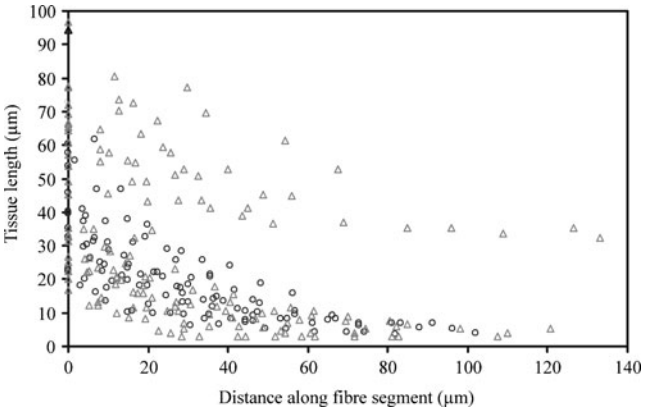

FIG. 5. Tissue length perpendicular to fiber segment plotted against distance from the fiber crossover for day 6 (circles) and 10 (triangles) of culture.

Tissue growth along the fiber segment

Tissue length along the fiber segment decreased with increasing distance from the fiber crossover. Plotting the measured data sets for day 6 and 10 highlighted different growth profiles along the fiber segment length (Fig. 5).

The day 6 data showed a clear exponential decrease in tissue growth along the fiber segment. A model of $\ln(f) = 6.5302 - 0.0219A - 0.0250FSd + 0.0138v$, with an R^2 value of 0.81, a SEE of 0.31 and a SECV of 0.32 were determined. This model is based on predicted values for the vertex tissue length, determined from the previously derived model. The small SEE, with closely matching SECV, indicated this model to predict data accurately. This showed that tissue growth along the fiber segment tended to be high for small to intermediate values of interfiber angle. The model $\ln(f) = 3.8612 - 0.0042A - 0.0237FSd$, with an R^2 value of 0.74 and a standard error of 0.36, also fits the data reasonably well and avoids the need for prediction of growth at the vertex.

The day 10 data appeared to be split into two groups, with upper and lower growth profiles, with the lower profile closely following that of day 6. The upper profile suggested increased tissue growth along the fiber segment when the tissue length near the fiber crossover was high, typically over 57 μm. Due to this split in the data, regression analysis is not presented for the day 10 data.

Visualization of predicted tissue growth

The visualization program showed models to predict tissue growth to a high level of accuracy in places (Fig. 6), indicated by the fit of the predicted tissue outline to that observed. Underprediction of tissue lengths was apparent (Fig. 6A), particularly where adjacent vertex tissue lengths crossed, as indicated by the crossing black lines in Figure 6B, with this interference predominantly due to short fiber segment lengths with neighboring acute interfiber angles.

Discussion

Understanding how scaffold architecture influences cellular activities leading to successful tissue engineering is the first step in optimizing scaffold design. Pore geometry plays a vital role in governing pore infiltration, with the shape of the pore dictating the distribution of cells within, and the resultant pattern of tissue growth.[18] In this study, we have correlated tissue growth within fiber-bound scaffold pores, with aspects of pore geometry, determining mathematical models for growth at fiber crossovers and along fiber segments.

Pore spanning was found to typically initiate at fiber crossovers, where interfiber distance was smallest. With increasing duration of culture pore infiltration continued from fiber segments, generally filling pores circumferentially. These observations in cell spanning and pore infiltration are in strong agreement with those of previous studies.[9,12,19] With increasing localized cell numbers spanning crossing fibers, with increased incubation time, cells remained in proximity of one another. This was likely to have aided further cell attachment through multiple sites, creating stability in the formed structure.

A lack of cell aggregates within pores (of modal length 26–50 μm) suggested cell spanning to have been relatively

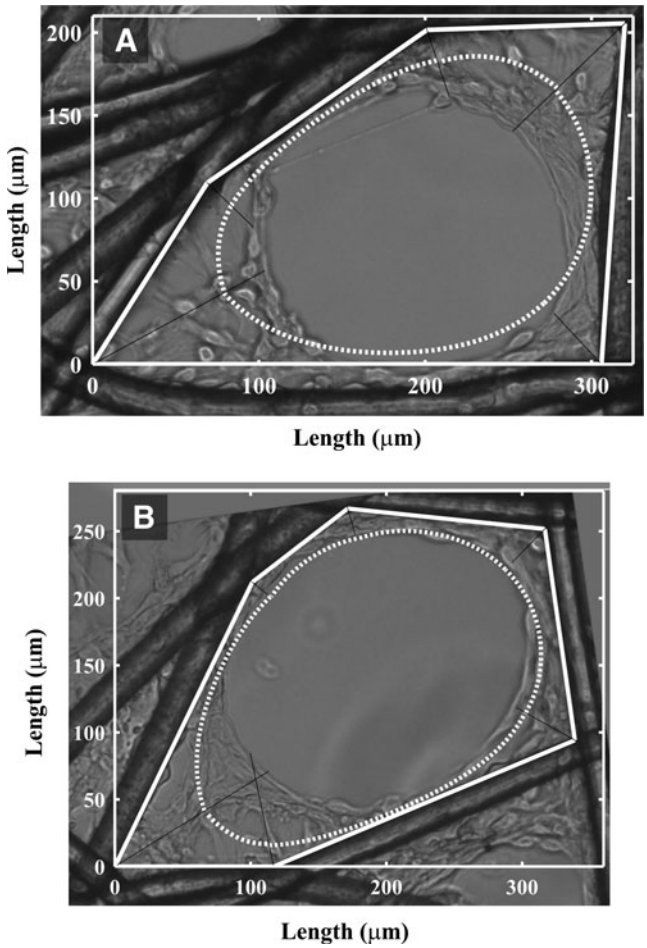

FIG. 6. (**A** and **B**) Visualization of predicted tissue growth in scaffold pores, with tissue outline (white dashed line) in pore boundary (solid white line). Black lines indicate actual vertex tissue lengths.

easy, with the formation of cell sheets, and cells remaining in their proliferative state. Previous studies found large cell aggregates to form within fiber-bound pores of slightly larger diameter (up to 76 μm).[5]

Characterizing tissue lengths at specific sites within pores gives an indication of the significance of that site on tissue growth, and how pore architecture might be improved for increased growth. Tissue lengths at fiber crossovers were found to decrease with increasing interfiber angle (an analogous study found comparable tissue lengths at similar interstrut angles).[12] Further to this, and previously unreported, we determined an exponential relationship between interfiber angle and tissue length. A possible explanation for this may be that cell spanning is easier at small interfiber angles, with spanning predominantly dependent on cell–strut interactions, with some cell–cell interactions. As the interfiber angle increases additional cell–cell interactions introduce further strain into the structure. Decreases in small interfiber angles may have reduced a larger number of these cell–cell interactions, compared to similar decreases in larger angles, creating more stability in the structure and the potential to grow longer tissue lengths.

Tissue lengths along fiber segments were found to decrease away from the fiber crossover, with the smallest lengths toward the fiber segment mid-point. The exponential decay pattern observed here was likely a consequence of decreased sites for cell attachment away from the fiber crossover. Analysis of the day 10 results suggests tissue growth to follow either the lower profile of day 6 or an upper profile. With increased cell numbers between the two timepoints, and no significant difference in vertex tissue lengths, one would have expected all day 10 profiles to follow the upper profile, layering on top of the already established cell layer of day 6. However, these results suggest that enhanced growth could only be achieved through sufficient tissue growth near the fiber crossover, supplying additional sites for cell attachment for continued growth along the fiber segment.

When used in conjunction, derived models were able to predict tissue growth within a scaffold pore on day 6 of culture. The developed visualization program presents a means of identifying the limitations of the derived models, by the fit between the actual tissue outline to the predicted outline. Underprediction of tissue lengths, particularly where tissue lengths cross, suggests other parameters, such as fiber segment length, may be an important consideration, and warrants inclusion in future models. The effect of fiber segment length was not found statistically significant in the present regression analyses; a more subtle combination of effects of the whole pore geometry may be at play. Obtaining a larger and wider range of data for analysis may enable more precise models for growth to be resolved. The in-house developed program presents a user-friendly means of visualizing the predicted tissue growth, based on the interfiber distances and interfiber angles constituting a pore. No other known methods of predicting tissue growth in pores based on pore geometry are known by the authors. Until now, only observations in the tissue pattern, in relation to pore geometry, have been reported.[18]

The approach developed in this work enables the prediction of tissue growth based on aspects of pore geometry, namely, the angle between crossing fibers and the distance between adjacent fiber crossovers. Considering this approach in the design of tissue engineering scaffolds, it is envisaged that tissue growth may, in part, be controlled by scaffold fiber orientation (dictating the interfiber angle) and packing density (controlling the distance between adjacent fibers).

One of the limitations of this approach is that three-dimensional tissue growth has been modeled two-dimensionally. However, with three-dimensional growth being an extension of two-dimensional growth, this is the first step in understanding tissue growth in relation to pore geometry. Future work should include using techniques such as microtomography to characterize three-dimensional tissue growth within three-dimensional scaffolds. Another limitation is that it is unclear how the derived mathematical models will change with different cell types. Cell types, such as keratinocytes and endothelial cells, are known to have different migratory behaviors,[3,12,16] which may result

in different mechanisms of cell spanning and pore infiltration. Compared to fibroblasts, which are known to be very motile, migrating either singularly or in groups, keratinocytes move slowly as an integrated sheet.[12] In spanning gaps fibroblasts take on an elongated morphology, whereas keratinocytes bridge distances by a process of stratification and are less elongated.[16] Future work will consider how models obtained for fibroblasts differ for those obtained using other cell types.

Conclusion

This study describes mechanisms of fibroblast spanning and pore infiltration within nonwoven scaffold pores. Further to this, and previously unreported, tissue growth at specific pore sites, at fiber crossovers, and along fiber segments has been characterized in terms of tissue length. On the basis of these measurements, mathematical models have been determined for tissue growth at particular time points during the proliferative phase of fibroblast culture. Incorporating these models into a software program enabled the visualization of predicted tissue growth. This approach presents a method for characterizing and predicting tissue growth in fiber-bound scaffold pores, identifying those aspects of pore geometry which are most important in pore infiltration. This approach will aid in the optimization of pore geometry, and scaffold structural engineering, for enhanced tissue growth.

Acknowledgments

E. Ingham and S.J. Russell are supported by the Leeds Centre of Excellence in Medical Engineering funded by the Wellcome Trust and EPSRC, WT088908/z/09/z.

Disclosure Statement

No competing financial interests exist.

References

1. Gomes, M.E., Holtorf, H.L., Reis, R.L., and Mikos, A.G. Influence of the porosity of starch-based fiber mesh scaffolds on the proliferation and osteogenic differentiation of bone marrow stromal cells cultured in a flow perfusion bioreactor. Tissue Eng **12,** 801, 2006.
2. Silva, M.M.C.G., Cyster, L.A., Barry, J.J.A., Yang, X.B., Oreffo, R.O.C., Grant, D.M., Scotchford, C.A., Howdle, S.M., Shakesheff, K.M., and Rose, F.R.A.J. The effect of anisotropic architecture on cell and tissue infiltration into tissue engineering scaffolds. Biomaterials **27,** 5909, 2006.
3. Salem, A.K., Stevens, R., Pearson, R.G., Davies, M.C., Tendler, S.J.B., Roberts, C.J., Williams, P.M., and Shakesheff, K.M. Interactions of 3T3 fibroblasts and endothelial cells with defined pore features. J Biomed Mater Res **61,** 212, 2001.
4. Edwards, S.L., Russell, S.J., Ingham, E., Matthews, J.B., and Mitchell, W. Nonwoven scaffolds of improved design for the tissue engineering of the anterior cruciate ligament. In: Anand, S.C., Kennedy, J.F., Miraftab, M., and Rajendran, S., eds. Medical Textiles and Biomaterials for Healthcare. Cambridge, United Kingdom: Woodhead Publishing Limited, 2006, pp. 355–365.
5. Ma, T., Li, Y., Yang, S.-T., and Kniss, D.A. Effects of pore size in 3D fibrous matrix on human trophoblast tissue development. Biotechnol Bioeng **70,** 606, 2000.
6. Ma, T., Li, Y., and Yang, S.-T. Tissue engineering human placenta trophoblast cells in 3-d fibrous matrix: spatial effects and cell proliferation and function. Biotechnol Prog **15,** 715, 1999.
7. Bashur, C.A., Dahlgren, L.A., and Goldstein, A.S. Effect of fiber diameter and orientation on fibroblast morphology and proliferation on electrospun poly (D,L-lactic-co-glycolic acid) meshes. Biomaterials **27,** 5681, 2006.
8. Chen, M., Patra, P.K., Lovett, M.L., Kaplan, D.L., and Bhowmick, S. Role of electrospun fiber diameter and corresponding specific surface area (SAA) on cell attachment. J Tissue Eng Regen Med **3,** 269, 2009.
9. Hutmacher, D.W., Schantz, T., Zein, I., Ng, K.W., Teoh, S.H., and Tan, K.C. Mechanical properties and cell cultural response of polycaprolactone scaffolds designed and fabricated via fused deposition modeling. J Biomed Mater Res **55,** 203, 2000.
10. Woodfield, T.B.F., Malda, J., de Wijn, J., Péters, F., Riesle, J., and van Blitterswijk, C.A. Design of porous scaffolds for cartilage tissue engineering using a three-dimensional fiber-deposition technique. Biomaterials **25,** 4149, 2004.
11. Wang, H., Pieper, J., Péters, F., van Blitterswijk, C.A., and Lamme, E. Synthetic scaffold morphology controls human dermal connective tissue formation. J Biomed Mater Res Part A **74A,** 523, 2005.
12. Sun, T., Smallwood, R., and MacNeil, S. Development of a mini 3D cell culture system using well defined nickel grids for the investigation of cell scaffold interactions. J Mater Sci Mater Med **20,** 1483, 2009.
13. O'Brien, F.J., Harley, B.A., Yannas, I.V., and Gibson, L.J. The effect of pore size on cell adhesion in collagen-GAG scaffolds. Biomaterials **26,** 433, 2005.
14. Ranucci, C.S., and Moghe, P.V. Polymer substrate topography actively regulates the multicellular organization and liver-specific functions of cultured hepatocytes. Tissue Eng **5,** 407, 1999.
15. Sun, T., Norton, D., McKean, R.J., Haycock, J.W., Ryan, A.J., MacNeil, S. Development of a 3D cell culture system for investigating cell interactions with electrospun fibers. Biotechnol Bioeng **97,** 1318, 2007.
16. Sun, T., Norton, D., Ryan, A.J., MacNeil, S., and Haycock, J.W. Investigation of fibroblast and keratinocyte cell-scaffold interactions using a novel 3D cell culture system. J Mater Sci Mater Med **18,** 321, 2007.
17. Berry, C.C., Campbell, G., Spadiccino, A., Robertson, M., and Curtis, A.S.G. The influence of microscale topography on fibroblast attachment and motility. Biomaterials **25,** 5781, 2004.
18. Engelmayr, G., Papworth, G.D., Watkins, S.C., Mayer, J.E., Jr., and Sacks, M.S. Guidance of engineered tissue collagen orientation by large-scale scaffold microstructures. J Biomech **39,** 1819, 2006.
19. Curtis, A.S.G., and Varde, M. Control of cell behavior: topological factors. J Natl Cancer Inst **33,** 15, 1964.
20. Edwards, S.L., Church, J.S., Werkmeister, J.A., and Ramshaw, J.A.M. Tubular micro-scale multiwalled carbon nanotube-based scaffolds for tissue engineering. Biomaterials **30,** 1725, 2009.

21. Folkman, J., and Moscona, A. Role of cell shape in growth control. Nature **273,** 345, 1978.
22. Singhvi, R., Kumar, A., Lopez, G.P., Stephanopoulos, G.N., Wang, D.I.C., Whitesides, G.M., and Ingber, D.E. Engineering cell shape and function. Science **264,** 696, 1994.
23. Chen, C.S., Mrksich, M., Huang, S., Whitesides, G.M., and Ingber, D.E. Geometric control of cell life and death. Science **276,** 1425, 1997.
24. ISO9073-1. Test methods for nonwovens—Part 1: Determination of mass per unit area. International Organization for Standardization of Standards, 1989.
25. ISO9073-2. Test methods for nonwovens—Part 2: Determination of thickness. International Organization for Standardization of Standards, 1995.

Address correspondence to:
Sharon L. Edwards, Ph.D.
Materials Science and Engineering
CSIRO
Henry Street
Belmont
Geelong
Victoria 3216
Australia

E-mail: sharon.edwards@csiro.au

Received: March 24, 2010
Accepted: July 30, 2010
Online Publication Date: September 27, 2010